JCEC
THE JOURNAL OF ENGINEERING AND EXACT SCIENCES

OPEN ACCESS

The Journal of Engineering and Exact Sciences – jCEC, Vol. 10 N. 02 (2024)
journal homepage: https://periodicos.ufv.br/jcec
eISSN: 2527-1075
ISSN: 2446-9416

Numerical simulation with hyperelastic constitutive model for high-performance multifilaments used in offshore mooring ropes

Article Info:
Article history: Received 2023-12-12 / Accepted 2024-01-20 / Available online 2024-01-25
doi: 10.18540/jcecvl10iss2pp17255

Daniel Magalhães da Cruz
ORCID: https://orcid.org/0000-0001-8734-0371
Federal University of Rio Grande do Sul, Mechanical Engineering Department, Brazil
E-mail: daniel.cruz@ufrgs.br
Tales Luiz Popiolek Júnior
ORCID: https://orcid.org/0000-0001-6733-3772
Federal University of Rio Grande, Engineering School, Brazil
E-mail: talespopiolekjr@furg.br
Marcelo de Ávila Barreto
ORCID: https://orcid.org/0000-0001-8796-8281
Federal University of Rio Grande, Engineering School, Brazil
E-mail: marcelobarretobm@gmail.com
Stephane Pires de Souza
ORCID: https://orcid.org/0009-0006-4421-4715
Federal University of Rio Grande, Engineering School, Brazil
E-mail: stephane.pires@outlook.com.br
Larissa Basei Zangalli
ORCID: https://orcid.org/0000-0002-7706-9271
Tecnofibers Desenvolvimento e Tecnologia Ltda, Brazil
E-mail: larissa@tecnofibers.com
Aleones José da Cruz Júnior
ORCID: https://orcid.org/0000-0003-0422-1911
Federal Institute of Education, Science and Technology Goiano, Brazil
E-mail: aleones.junior@ifgoiano.edu.br
Taline Carvalho Martins
ORCID: https://orcid.org/0000-0002-1496-296X
Federal Institute of Education, Science and Technology Goiano, Brazil
E-mail: taline.carvalho@ifgoiano.edu.br
Ana Lúcia Nazareth da Silva
ORCID: https://orcid.org/0000-0002-7668-2576
Rio de Janeiro Federal University, Macromolecule Institute Professor Eloisa Mano (IMA) and Environmental Engineering Program (PEA), Brazil
E-mail: ananazareth@ima.ufrj.br
Ivan Napoleão Bastos
ORCID: https://orcid.org/0000-0001-7611-300X
Rio de Janeiro State University, Polytechnic Institute, Brazil
E-mail: inbastos@iprj.uerj.br
Carlos Eduardo Marcos Guilherme
ORCID: https://orcid.org/0000-0001-5356-6524
Federal University of Rio Grande, Engineering School, Brazil
E-mail: carlosguilherme@furg.br

Abstract
The present study addresses the numerical simulation of the stress-strain behavior of synthetic multifilaments subjected to creep, fatigue cycles, and rupture. Understanding the mechanical properties of these materials is essential for various industrial applications, including technical textiles, ropes, cables, and composite materials. In this study, advanced simulation methods are employed using concepts from continuum mechanics and solid mechanics, coupled with a hyperelastic model. The simulated materials are high modulus polyester and polyethylene fibers for use in multifilament structures. Experimental tests were conducted to validate the simulation, and the simulation results were compared to the reference data to assess the quality of the numerical simulation. As a result, the numerical modeling shows capable of representing the constitutive behavior under creep, fatigue, and rupture solicitations. There was a certain difficulty in representing the behavior when many inelastic components were present in the fibers. Additionally, changes in curvature and concavity pose challenges that could potentially be addressed by other energy models integrated into the proposed code. These findings have significant implications in engineering sectors.
Keywords: Numerical assessment. Polyester fibers. HMPE fibers. Stress-strain behavior. Hyperelastic model. Viscoelasticity.

Nomenclature

$\overline{I_1}$	Invariant 1, continuum mechanics made for the isochoric parcel
$\overline{I_2}$	Invariant 2, continuum mechanics made for the isochoric parcel
$\overline{I_3}$	Invariant 3, continuum mechanics made for the isochoric parcel
$\overline{\boldsymbol{F}}^T$	Transposed of the deformation gradient, refers to the isochoric parcel
$\mathbb{R}^3$	Real space, three-dimensional coordinates
C_1, C_2, C_3	Model constants
I_1	Invariant 1, continuum mechanics
I_2	Invariant 2, continuum mechanics
I_3	Invariant 3, continuum mechanics
$\overline{\boldsymbol{C}}$	Modified tensor for right isochoric Cauchy-Green parcel
$\overline{\boldsymbol{F}}$	Deformation gradient, referring to the isochoric parcel
$\widehat{\boldsymbol{F}}$	Deformation gradient, refers to the volumetric parcel
$\boldsymbol{F}^T$	Transpose of the deformation gradient
$\tilde{\boldsymbol{S}}$	Second Piola-Kirchhoff stress tensor, referring to the isochoric parcel
γ_∞	Model stiffness parcel
ρ_L	Linear density
σ_{exp}	Experimental stress
σ_{num}	Numerical stress
$\boldsymbol{\sigma}_{n+1}$	Standard transformation (push-forward) for the Kirchhoff stress tensor (spatial)
Δt	Variation in time, or step in time
°	Deviatoric function indication
ASTM	American Society for Testing and Materials
denier	Linear density unit (1 tex = 9 denier)
det	Determinant
dev	Deviatoric function
dtex	Linear density unit, decitex submultiple of tex
HMPE	High Modulus Polyethylene
ISO	International Organization for Standardization
MODU	Mobile Offshore Drilling Units
PET	Polyester, Poly(ethylene terephthalate)
tex	Linear density unit, with g/km unit
tr	Trace of a matrix

YBL	Yarn break load
Ω	Real body
J	Jacobian
W	Energy function
i	Counter structure
n	Previous time, previous step
$n+1$	Current time, current step
$\boldsymbol{B}$	Left Cauchy-Green deformation tensor
$\boldsymbol{C}$	Right Cauchy-Green deformation tensor
$\boldsymbol{F}$	Deformation gradient
$\boldsymbol{H}$	Parameter created in the mathematical model, internal variable
$\boldsymbol{I}$	Identity matrix
$\boldsymbol{S}$	Second Piola-Kirchhoff stress tensor
$\boldsymbol{X}$	Material point in reference
τ	Material property
φ	Finite deformation
ψ	Relative percentage difference
ϵ	Average error

1. Introduction

In recent decades, materials engineering has progressed significantly, driving growth in academic research, industrial production, technological applications, and commercialization of polymers, particularly fibers. These polymers are increasingly cost-effective and often possess superior properties compared to natural materials (Callister Jr, 2008; Hage Jr, 1998).

Polymers excel in applications with characteristics such as low density, substantial toughness (at times on pair with metals), effective vibration damping, low friction coefficients, thermal insulation capabilities, and notable corrosion resistance (Mckenna et al., 2004). An example of their utility is evident in offshore mooring systems, where synthetic fiber ropes have supplanted conventional steel cables due to their enhanced performance in marine conditions and reduced weight (Del Vecchio, 1992; Haach et al., 2010).

The continuous evolution of these mooring ropes aims to confer greater stiffness to limit the movement of floating units, making the study of their mechanical performance a fundamental field (Barrera et al., 2019; da Cruz et al., 2023; Liu et al., 2014). The synthetic polymeric multifilaments used in these ropes can be composed of various materials, with polyester and high modulus polyethylene (HMPE) standing out. Polyester is widely employed in offshore mooring systems and has a solid foundation of literature studies (Bosman & Hooker, 1999; Del Vecchio, 1992; Flory et al., 2007; Wibner et al., 2003). On the other hand, high modulus polyethylene, despite being more recent and costly, exhibits excellent mechanical performance and has been studied for use in Mobile Offshore Drilling Units (MODU) and other mooring applications (Berryman et al., 2002; Leite & Boesten, 2011; Lian et al., 2017; Vlasblom et al., 2012).

Mechanical characterization of polymeric materials emphasizes studying multifilament construction, which is influenced by variables like temperature, humidity, and mechanical loads. Due to the nonlinear nature of these materials, predicting their behavior poses a complex challenge (Louzada et al., 2017). Consequently, much research relies on experimental data (Belloni et al., 2021; da Cruz et al., 2022a; da Cruz et al., 2023; Melito et al., 2022; Sry et al., 2017; Xu et al., 2020). Analyzing material mechanics is crucial for understanding and foreseeing structural performance across applications. In the realm of synthetic fibers, like polyester and HMPE, characterizing responses under different load conditions—rupture, creep, and fatigue—is pivotal for ensuring the safety and durability of various products and structures.

Numerical simulation becomes a potent means for exploring the inherent behavior of these materials under diverse loads. Numerous studies in literature use this computational approach to

examine mechanical performance in scenarios challenging or infeasible for real experiments (Chen et al., 2023; Cifuentes et al., 2015; Tang et al., 2020; Tsukrov et al., 2005; Yuan et al., 2014). Furthermore, numerical simulation provides valuable insights by unveiling intricate details about stress, deformation, and other internal variables that may not be readily observable through experimentation. Different works in the literature address this constitutive framework that numerical predicts the stress-strain response under loading conditions (da Cruz et al., 2022b; Danielsson et al., 2004; Sedighiani et al., 2020; Stumpf et al., 2023; Wang et al., 2022).

This article aims to analyze the constitutive behavior of polyester and HMPE fibers for offshore use through numerical simulation under different load types by using polymeric fibers with offshore moorings experiments and numerical approaches. Experimental data were utilized to validate the numerical simulation. The numerical simulation is based on continuum mechanics and a hyperelastic model, considering viscoelastic behavior. Simulated loads include rupture, creep, and fatigue. Understanding the constitutive behavior of polyester and HMPE fibers under creep, fatigue, and rupture conditions, combined with numerical simulations and experimental analyses allowed to validate the modeling capability. It is important to highlight that this study is innovative in offshore mooring ropes applications.

2. Materials and Methods

2.1 Fiber Specification

The study uses polyester (PET) and high modulus polyethylene (HMPE) multifilaments, both used in the manufacture of offshore mooring ropes and coming from spools. About specifications, ~~the~~ PET is coded as SFS5202, with a specific mass of 1.38 g/cm³ and an indicated linear density of 2000 denier (2200 dtex). On the other hand, the HMPE is coded as JX99, with a specific mass of 0.97 g/cm³ and a linear density of 1600 denier (1780 dtex) for the multifilament. Figure 1 depicts the spools of both materials.

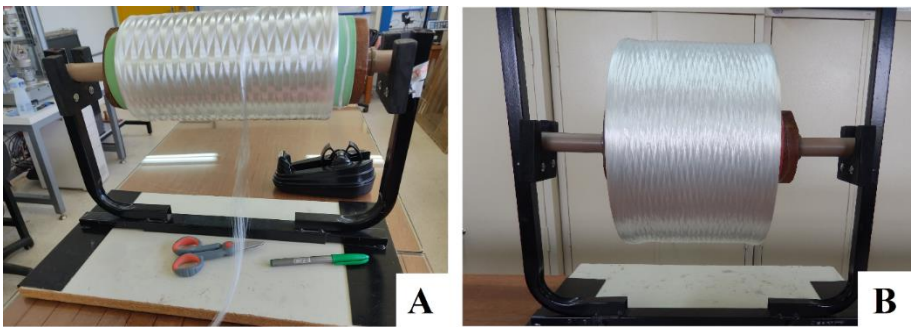

Figure 1 – Spools: (A) High modulus polyethylene; (B) Polyester.

In the tensorial framework, data is processed as stress; however, in the multifilament tests, measuring the actual area is a challenge, making it impossible to rely on stress calculations using the conventional load-to-area ratio. Therefore, a mathematical approach is employed that combines load, density (ρ), and linear density (ρ_L) to determine the stress (σ), as described in Equation 1.

$$\sigma[MPa] = \frac{F[N] \cdot \rho\left[\frac{g}{cm^3}\right]}{\rho_L\left[\frac{g}{m}\right]} \quad (1)$$

2.2 Experimental

Numerical simulation incorporates experimental data for creep, fatigue (loading and unloading), and rupture data. Additionally, a previous characterization of the samples is necessary in terms of linear density, Yarn Break Load (YBL), linear tenacity, and rupture elongation. The experimental tests conducted for the polyester and HMPE fibers include: linear density (or title), break test (Yarn Break Load – YBL), creep, and fatigue.

Linear density was measured following the ASTM D1577 standard using a precision balance. Standard 1000 mm samples stabilized for 9 minutes before mass recording, with ten samples per fiber type.

Yarn Break Load (YBL) test was conducted on the Instron 3365 universal testing machine, as shown in Figure 2a, following ISO 2062 procedures. Using 500-mm length specimens with a twist rate of 60 turns/m, an extension rate of 250 mm/min was determined the break strength and extension (final elongation). Fifteen samples were tested per fiber, contributing to initial multifilament characterization and subsequent numerical simulation for each material.

The creep rupture test adheres to ISO 18692-2 for polyester and ISO 18692-3 for HMPE, performed on the Instron 3365 (Figure 2a). The test conditions involve stress load and time-stop parameter, with the reference value being the YBL of each multifilament. The test group for creep rupture is at 80% of the YBL, using 500-mm sample length with a twist rate of 60 turns/m. A ramp leads to the creep force level, using a smooth ramp with a rate of 250 N/min under force control.

The fatigue test occurs on the Instron E-3000 (Figure 2b), with force-based control and cyclic load. It involves a maximum load of 45% of YBL and a minimum load of 0% (zero load). Each specimen underwent one hundred fatigue cycles at a frequency of 0.10 Hz, resulting a total test time of 1000 seconds, for the 200-mm specimen length.

Throughout the multifilament tests, temperature remained at 20±2 °C, and relative humidity was 65±4%, conforming to the ISO 139 atmospheric fiber testing standard.

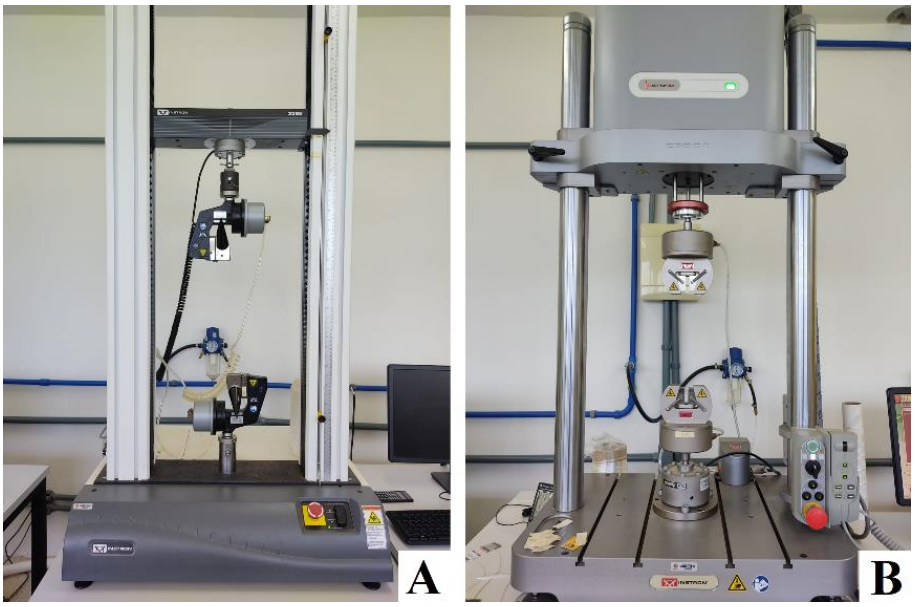

Figure 2 – Tensile apparatus: (A) Instron 3365 (YBL and creep rupture test); (B) Instron E-3000 (fatigue test).

2.3 Tensor Mathematics Methodology

The numerical code was developed based on Simo and Hughes (1997), Cruz (2022) and Cruz et al. (2023), using the MathWorks Inc. MATLAB platform. The mathematical formulation relies on the elasticity theory and the properties of the material under analysis.

Considering a body $\Omega \subset \mathbb{R}^3$, subjected to finite deformation $\varphi: \Omega \rightarrow \mathbb{R}^3$, the deformation gradient $\boldsymbol{F} = \partial\varphi(\boldsymbol{X})/\partial\boldsymbol{X}$ is defined where $\boldsymbol{X}$ is the material point in the reference (undeformed) configuration, and $J = \det \boldsymbol{F} > 0$ is the Jacobian. The deformation gradient $\boldsymbol{F}$ can be multiplicatively decomposed (Flory, 1961), as shown in Equation 2. Where $\widehat{\boldsymbol{F}}$ refers to the volumetric part and $\overline{\boldsymbol{F}}$ refers to the isochoric part, respectively defined in Equation 3 and Equation 4. The variable $\boldsymbol{I}$ corresponds to the identity matrix.

$$\boldsymbol{F} = \widehat{\boldsymbol{F}}\overline{\boldsymbol{F}} \tag{2}$$

$$\widehat{\boldsymbol{F}} = J^{1/3}\boldsymbol{I}, \text{ with } \det\widehat{\boldsymbol{F}} = \det\boldsymbol{F} = J \tag{3}$$

$$\overline{\boldsymbol{F}} = J^{-1/3}\boldsymbol{F}, \text{ with } \det\overline{\boldsymbol{F}} = 1 \tag{4}$$

From Equation 2, the right Cauchy-Green tensor in the isochoric term ($\overline{\boldsymbol{C}}$) can be written in terms of $\overline{\boldsymbol{C}} = \overline{\boldsymbol{F}}^T\overline{\boldsymbol{F}} = J^{-2/3}\boldsymbol{C}$. With $\det\overline{\boldsymbol{C}} = 1$ and $\boldsymbol{C} = \boldsymbol{F}^T\boldsymbol{F}$, the invariants of $\overline{\boldsymbol{C}}$ are determined in Equations 5, 6, and 7.

$$\overline{I_1} = tr\,\overline{\boldsymbol{C}} \tag{5}$$

$$\overline{I_2} = \frac{1}{2}((tr\,\overline{\boldsymbol{C}})^2 - tr\,\overline{\boldsymbol{C}}^2) \tag{6}$$

$$\overline{I_3} = \det\overline{\boldsymbol{C}} = 1 \tag{7}$$

An internal variable ($\boldsymbol{H}$) is introduced from material properties (τ_i), time step (Δt_n), and Piola-Kirchhoff stress tensor ($\tilde{\boldsymbol{S}}$). Mathematical advancement involves optimization loops for refining energy model constants (C_i) and the tensorial script. The internal variable $\boldsymbol{H}$ updating equation is in Equation 8. Tensor $\boldsymbol{S}$ is defined in Equation 9.

$$\boldsymbol{H}_{n+1} = \exp(-\Delta t_n/\tau_i)\boldsymbol{H}_n + \exp(-\Delta t_n/2\tau_i)\left(\tilde{\boldsymbol{S}}_{n+1} - \tilde{\boldsymbol{S}}_n\right) \tag{8}$$

$$\boldsymbol{S} = 2\left[\frac{\partial W}{\partial I_1} + \frac{\partial W}{\partial I_2}\right]\boldsymbol{I} - 2\frac{\partial W}{\partial I_2}\boldsymbol{C} + 2\frac{\partial W}{\partial I_3}I_3\boldsymbol{C}^{-1} \tag{9}$$

In Equation 9, W is the energy function. In the literature, there are various energy models, both phenomenological and micromechanical. For this study, the two-term Mooney-Rivlin model is used (Mooney, 1940; Rivlin, 1956), as shown in Equation 10. This model is oriented towards isotropic and hyperelastic materials, and was chosen because it is a classic model, with wide application and low computational processing cost (few coefficients to optimize). This model is phenomenological, linearly dependent on the first and second invariant, and is perhaps the most celebrated among the classical hyperelastic models (Hoss, 2009).

$$W = C_1(I_1 - 3) + C_2(I_2 - 3) \tag{10}$$

Deviatoric functions are calculated for the second Piola-Kirchhoff stress tensor and for the internal variable. Equation 11 shows the mathematical form of calculating this deviatoric function. It is noteworthy that the operation in brackets in Equation 11 is an inner product, which can be defined as the trace of the inverse of ■ with $\boldsymbol{C}$. The superscript '°' indicates the execution of a deviatoric function.

$$DEV_{n+1}(\blacksquare) = (\blacksquare) - (1/3)\cdot[(\blacksquare):\boldsymbol{C}_{n+1}]\boldsymbol{C}_{n+1}^{-1} \tag{11}$$

The deviatoric functions associated with the stiffness model of the system provide a final stress matrix, based on Equation 12, where '°' indicates the deviatoric function. Simo and Hughes (1997) define that $\gamma_\infty = \gamma - 1$, which corresponds to a stiffness portion of the model. Thus, Equation 12 is rewritten as Equation 13.

$$\boldsymbol{S}_{final} = \gamma_\infty \cdot \boldsymbol{S}^\circ_{n+1} + \gamma \cdot \boldsymbol{H}^\circ_{n+1} \tag{12}$$

$$\boldsymbol{S}_{final} = (\gamma - 1) \cdot \boldsymbol{S}^{\circ}_{n+1} + \gamma \cdot \boldsymbol{H}^{\circ}_{n+1} \quad (13)$$

For the final stress expression, as comparing the second Piola-Kirchhoff tensor is impractical, a stress transformation is performed to allow result comparison. Thus, the Kirchhoff (spatial) stress tensor is calculated through the standard transformation, Equation 14. From the stress already transformed, deformations and stresses are extracted for plotting.

$$\boldsymbol{\sigma}_{n+1} = \boldsymbol{F}_{n+1} \boldsymbol{S}_{final} \boldsymbol{F}^{T}_{n+1} \quad (14)$$

To assess the convergence of results, it is necessary to quantify the error. The relative percent difference (ψ) between the experimental and numerical values is calculated using Equation 15, and then an average error (ϵ) is determined Equation 16.

$$\psi[\%] = \left(\frac{\sigma_{num} - \sigma_{exp}}{\sigma_{exp}} \right) \cdot 100 \quad (15)$$

$$\epsilon[\%] = \frac{|\sum \psi_i|}{i} \quad (16)$$

3. Results and Discussions

3.1 Experimental

The initial characterization results of PET and HMPE multifilaments are shown in Table 1. In the presented data, it is noteworthy that the tenacity of HMPE conforms to ISO 18692-3 standard (should be higher than 2.5 N/tex). Additionally, several studies on fibers at the same construction level (multifilaments) exhibit similar orders of magnitude for both polyester and high modulus polyethylene (Belloni et al., 2021; Camargo et al., 2016; Chimisso, 2009; da Cruz et al., 2022a; Hahn et al., 2022; Stumpf et al., 2023; Weller et al., 2015).

Table 1 – Initial characterization results: Polyester and HMPE.

	Polyester (PET)	HMPE
Linear density [dtex]	2273	1812
Breaking strength [N]	182	561
Breaking stress [MPa]	1084	3001
Elongation at break [mm]	66.15	14.90
Deformation at break [%]	13.23	2.98
Linear tenacity [N/tex]	0.80	3.09

The experimental rupture data are already compiled in Table 1. The rupture data will be used for calibrating the numerical simulation. For this purpose, among the tested specimens, the one closest to the average values was selected, and this representative specimen is used for calibration and numerical simulation. Figure 3 illustrates the rupture test of the representative specimen for both polyester and HMPE.

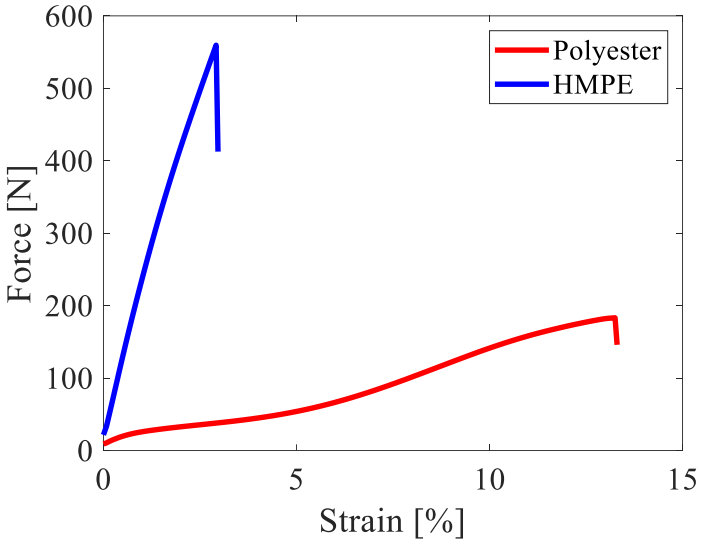

Figure 3 – Experimental rupture test.

The experimental creep rupture results are categorized in terms of time and deformations and are presented in Table 2. It is important to note that numerical simulation deals with the constitutive behavior, which involves stress-strain information. Therefore, it does not rely on time-related data or even the conventional creep test. Nevertheless, as an experimental outcome, the creep results for polyester and HMPE is displayed in Figure 4.

Table 2 – Results of the creep rupture tests for applied loads of 80% of the YBL.

	Polyester (PET)	HMPE
Creep time [s]	1713	1613
Rupture time [s]	1746	1716
Creep deformation [%]	1.71	2.51
Rupture deformation [%]	12.21	5.23

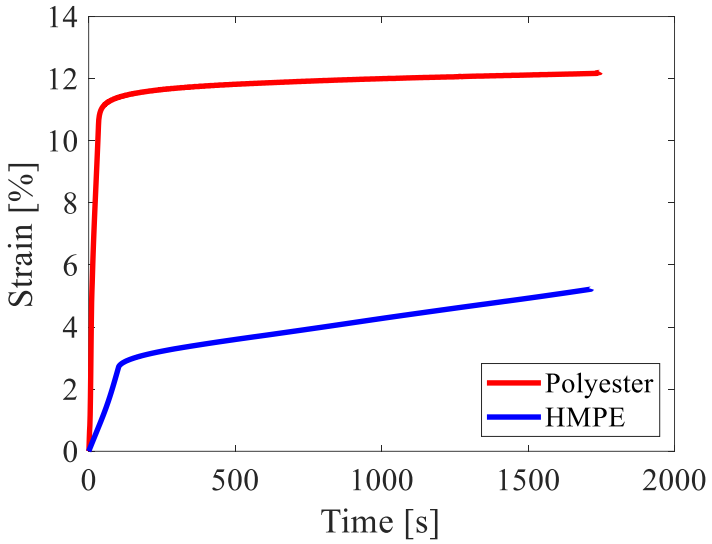

Figure 4 – Experimental creep test at 80% of the YBL.

The results from Figure 3, Figure 4 and Table 1 show that HMPE is more rigid compared to polyester (PET) material, which presented a higher deformation capacity. This behavior will also be evident in the fatigue test, which will be analyzed below.

For the fatigue test, control is maintained overload, specific frequency, and the number of cycles for the test. The primary response is in terms of gradual deformation over the cycles. While only the last fatigue cycle (hundredth cycle) is simulated for numerical purposes, the experimental results of fatigue-induced deformation for polyester and HMPE in Figure 5.

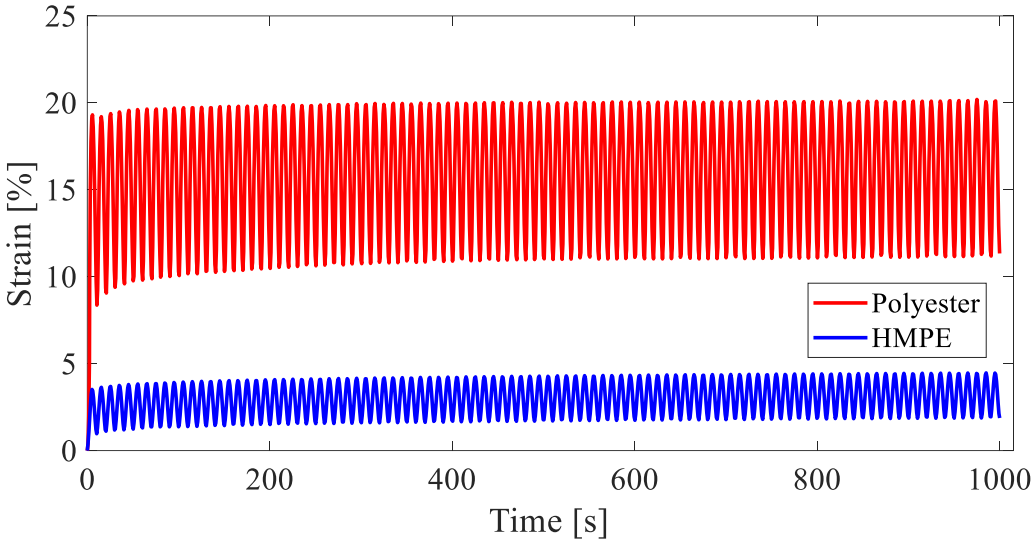

Figure 5 – Experimental fatigue: 100 cycles for polyester and HMPE under 0 - 45% YBL loading.

In the graph presented in Figure 5, the removal of inelastic portions in both materials is evident in the strain over the loading and unloading cycles, with a more pronounced effect observed in the polyester. In other words, both viscoelastic materials exhibit inelastic portions that are removed through cycling. As more cycles are conducted, the behavior becomes more homogeneous, strain stabilizes, and if a stress-strain graph were plotted, it would approach a hysteresis curve. Polyester exhibits a higher quantity of inelastic portions when compared to HMPE, as well as a greater viscoelastic characteristic, as demonstrated in Figure 3.

3.2 Numerical Simulation

For numerical results of the different load conditions applied in the numerical routine, the constants for all simulations are provided in Table 3.

Table 3 – Numerical simulation constants.

	Rupture		**Creep**		**Fatigue cycle**	
	PET	HMPE	PET	HMPE	PET	HMPE
γ	0.500	0.500	0.500	0.500	0.500	0.500
τ	3597.031	731.913	78.533	69.453	22.680	160.292
C_1	4.108	162.798	1.370	65.231	21.153	218.432
C_2	0.013	9.087	6.151×10^{-4}	1.225	8.001×10^{-8}	1.640×10^{-6}

When considering the numerical results obtained from the simulation and optimization of the constants, it becomes challenging to discern a consistent pattern. This difficulty arises from the fact that the behavior exhibited is not uniform, both concerning the mechanical tests and the material properties. This is further complicated by the use of a phenomenological model. But some numerical values and relationships draw attention in certain aspects. If the values of constants C_1 and C_2 are observed, for each of the mechanical load conditions, comparing the values between PET and HMPE, it is observed that the values for polyester in these constants are significantly lower when compared to HMPE.

Another value that draws attention is the γ, which for all mechanical tests and all materials remains the same at 0.500. Although it is a dimensionless value that belongs to system modeling, this specific value offers an interpretation of something equivalent to a stiffness portion of a relationship between the system and the material. Its origin comes from the use of the generalized Maxwell model (Simo and Hughes, 1997), although it is not explored in the present study, it indirectly infers that this equal value for all simulations is linked to the viscous and non-linear characteristics of the material.

The results of the numerical simulations are displayed in figures for PET and HMPE. Each plot includes the curve obtained through numerical simulation and discrete experimental data. Figure 6 presents the numerical simulations for rupture. Figure 7 depicts the graphical numerical outcomes for creep. Lastly, Figure 8 shows the simulations for the loading and unloading cycles (fatigue).

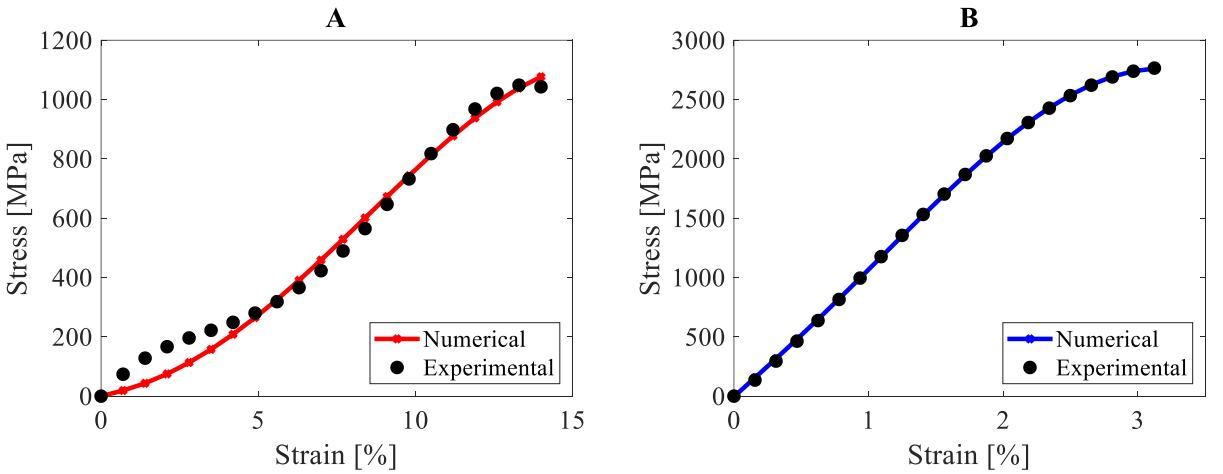

Figure 6 – Numerical and experimental results for rupture: (A) PET; (B) HMPE.

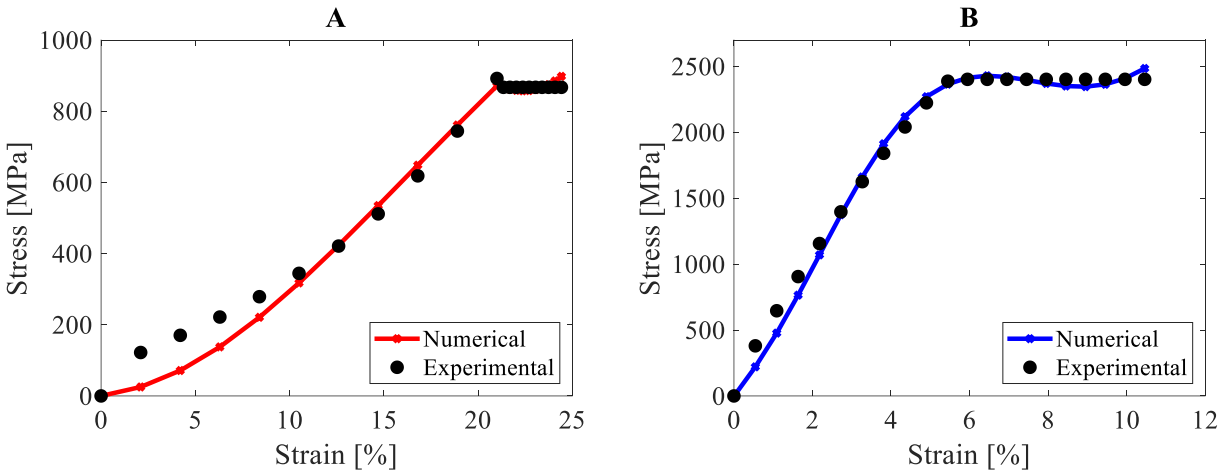

Figure 7 – Numerical and experimental results for creep: (A) PET; (B) HMPE.

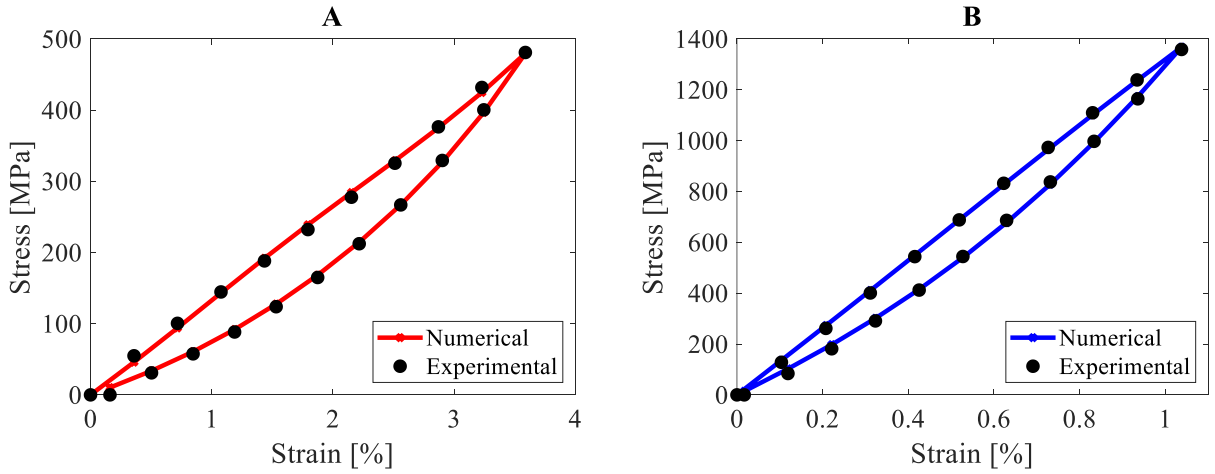

Figure 8 – Numerical and experimental data for the 100th fatigue cycle: (A) PET; (B) HMPE.

The most visually compelling results are evident in the fatigue cycle, as well as in the rupture of HMPE. Nevertheless, the outcomes remain well satisfactory, even in cases where there is less agreement between the numerical simulation and experimental data.

The numerical simulation of rupture behavior of PET, along with its ramp in creep, is noteworthy. The model encounters difficulty in capturing changes in the data curvature, especially shifts in concavity. Considering the good fatigue results, this observation gains significance. These robust fatigue results arise numerical simulation from testing the hundredth cycle under high load amplitude.

Specifically for the loading and unloading test, during the previous 99 cycles (although not numerically simulated), the cycling eliminates the inelastic deformation of both fibers, thus homogenizing the behavior of the curve. Thus, the behavior of the hundredth cycle, which is simulated numerically, is stable, with a graphical behavior close to a hysteresis loop. In the literature, there are studies for synthetic fibers that precisely show these non-linear characteristics, and the inelastic removal by fatigue and its effect in the stiffness (Chevillotte et al., 2020; Huang et al., 2013; Melito et al., 2022; Nguyen and Thiagarajan, 2022; Pham et al., 2019; Sørum et al., 2023; Włochowicz et al., 2016).

Homogenization of the curve by removing inelastic portions does not produce a linear fatigue behavior of the stress-strain relationship. Curvature persists in the fatigue response, also revealing some non-coincidence in load and unload data. The crucial aspect is that despite curvature adjustments, the behavior remains homogenous with just one concavity. The mathematical criterion for quantifying the error is applied to all simulations, compared to experimental. Table 4 presents the average errors expressed as percentages.

Table 4 – Average error (ϵ) of numerical simulations, in percentage [%].

	Polyester (PET)	HMPE
Rupture	16.15	1.44
Creep	10.93	5.67
Fatigue cycle	3.01	2.79

4. Conclusions

The mechanical tests showed different behaviors between PET and HMPE materials used in mooring rope applications.

Numerical simulation plays a pivotal role in comprehending the stress-strain behavior of synthetic multifilaments under various loading conditions. The script developed in this study captures the constitutive behavior concerning rupture, creep, and fatigue, offering a valuable tool for predicting and optimizing multifilament performance to technological applications.

This investigation delves into the intricacies of material properties, load impacts, and their influence on numerical mechanical responses. Key trends emerge, such as the consistent global stiffness alignment (represented as γ) and the magnitudes of simulated constants. Using advanced computational models, we have successfully explored complex scenarios, with the exception of polyester rupture, where average errors exceeded 10%. These findings underscore the critical role of simulation in ensuring multifilament safety and reliability across diverse load conditions, highlighting the importance of both macroscopic factors such as maximum stress and strain, as well as microscopic aspects encompassing filament interactions and internal failures.

Remarkably, the most substantial reduction in errors is observed in load cycling simulations, where inelastic fiber parcels have minimal effects. However, to make further advancements, it is necessary to enhance simulation models to incorporate greater realism, accounting for material variations, environmental influences, and geometric complexities. Experimental validation remains an essential guiding principle for future research endeavors. The integration of additional models that can better capture curvature and concavity modifications holds promise for achieving even smaller errors in representing the constitutive behavior of multifilaments. The numerical simulation and experimental validation can undoubtedly continue to advance our understanding and prediction of multifilament behavior in various industrial and technological contexts.

Acknowledgements

This study was financed in part by the Coordenação de Aperfeiçoamento de Pessoal de Nível Superior – Brasil (CAPES) – Finance Code 001, besides Conselho Nacional de Desenvolvimento Científico e Tecnológico – CNPq (Grant n° 307889/2022).

References

ASTM, American Society for Testing and Materials. (2018), *D1577 - Standard Test Methods for Linear Density of Textile Fibers*. West Conshohocken: ASTM International.

Barrera, C., Guanche, R., & Losada, I. J. (2019). Experimental modelling of mooring systems for floating marine energy concepts. *Marine Structures*, *63*, 153-180. https://doi.org/10.1016/j.marstruc.2018.08.003.

Belloni, E. da S., Clain, F. M., & Guilherme, C. E. M. . (2021). Post-impact mechanical characterization of HMPE yarns. *Acta Polytechnica*, *61*(3), 406–414. https://doi.org/10.14311/AP.2021.61.0406.

Berryman, C. T., Dupin, R. M., & Gerrits, N. S. (2002). Laboratory study of used HMPE MODU mooring lines. In *Offshore Technology Conference* (OTC-14245). https://doi.org/10.4043/14245-MS.

Bosman, R. L. M., & Hooker, J. (1999). The elastic modulus characteristics of polyester mooring ropes. In *Offshore Technology Conference* (OTC-10779). https://doi.org/10.4043/10779-MS.

Callister Jr, W. D. (2008). *Ciência e engenharia de materiais: uma introdução*, 7ª ed., Livros Técnicos e Científicos Editora SA, Rio de Janeiro.

Camargo, F. V., Guilherme, C. E. M., Fragassa, C., & Pavlovic, A. (2016). Cyclic stress analysis of polyester, aramid, polyethylene and liquid crystal polymer yarns. *Acta Polytechnica*, *56*(5), 402-408. https://doi.org/10.14311/AP.2016.56.0402.

Chen, M., Li, C. B., Han, Z., & Lee, J. B. (2023). A simulation technique for monitoring the real-time stress responses of various mooring configurations for offshore floating wind turbines. *Ocean Engineering*, *278*, 114366. https://doi.org/10.1016/j.oceaneng.2023.114366.

Chevillotte, Y., Marco, Y., Bles, G., Devos, K., Keryer, M., Arhant, M., & Davies, P. (2020). Fatigue of improved polyamide mooring ropes for floating wind turbines. *Ocean Engineering*, *199*, 107011. https://doi.org/10.1016/j.oceaneng.2020.107011.

Chimisso, F. E. (2009). Some experimental results regarding creep behavior on synthetic materials used to produce offshore morring ropes. *Strain*, *3*(3.24), 12-67.

Cifuentes, C., Kim, S., Kim, M. H., & Park, W. S. (2015). Numerical simulation of the coupled dynamic response of a submerged floating tunnel with mooring lines in regular waves. *Ocean Systems Engineering*, *5*(2), 109-123. https://doi.org/10.12989/ose.2015.5.2.109.

Cruz, D. M. (2022), *Estudo teórico, experimental e numérico do comportamento viscoelástico e caracterização de fibras sintéticas poliméricas*. Trabalho de Conclusão de Curso de graduação em Engenharia Mecânica, Universidade Federal do Rio Grande. Rio Grande, Brasil. http://argo.furg.br/?RG001477614.

Cruz, D. M. da, Popiolek Júnior, T. L., Barreto, M. de Ávila, Guilherme, C. E. M., & Stumpf, F. T. (2023). Avaliação de modelos de energia para simulação numérica do comportamento mecânico de multifilamentos de poliéster. *The Journal of Engineering and Exact Sciences*, *9*(1), 15321–01e. https://doi.org/10.18540/jcecvl9iss1pp15321-01e.

da Cruz, D. M., Clain, F. M., & Guilherme, C. E. M. (2022a). Experimental study of the torsional effect for yarn break load test of polymeric multifilaments. *Acta Polytechnica*, *62*(5), 538–548. https://doi.org/10.14311/AP.2022.62.0538.

da Cruz, D. M., Guilherme, C. E. M., Stumpf, F. T., & Bastos, M. B. (2022b, April). Numerical Assessment of Mechanical Behavior of Mooring Lines Using Hybrid Synthetic Fiber-Rope Segments. In *Offshore Technology Conference*. OnePetro. https://doi.org/10.4043/31906-MS.

da Cruz, D. M., Penaquioni, A., Zangalli, L. B., Bastos, M. B., Bastos, I. N., & da Silva, A. L. N. (2023). Non-destructive testing of high-tenacity polyester sub-ropes for mooring systems. *Applied Ocean Research*, *134*, 103513. https://doi.org/10.1016/j.apor.2023.103513.

Danielsson, M., Parks, D. M., & Boyce, M. C. (2004). Constitutive modeling of porous hyperelastic materials. *Mechanics of Materials*, *36*(4), 347-358. https://doi.org/10.1016/S0167-6636(03)00064-4.

Del Vecchio, C. J. M. (1992). *Lightweight materials for deep water moorings* (Doctoral dissertation, University of Reading, U.K.).

Flory, J. F., Banfield, S. J., & Berryman, C. (2007). Polyester mooring lines on platforms and MODUs in deep water. In *Offshore Technology Conference* (OTC-18768). https://doi.org/10.4043/18768-MS.

Flory, P. (1961). Thermodynamic relations for high elastic materials. *Transactions of the Faraday Society*, *57*, 829-838.

Haach, L. F., Poitevin, D. T., & Bastos, M. B. (2010). Prospects of synthetic fibers for deepwater mooring. In *Proceedings of the Rio Oil and Gas Expo and Conference*, Rio de Janeiro, Brazil.

Hage Jr, E. (1998). Aspectos Históricos sobre o Desenvolvimento da Ciência e da Tecnologia de Polímeros. *Polímeros*, *8*, 6-9. https://doi.org/10.1590/S0104-14281998000200003.

Hahn, G., Monteiro da Fonseca Thomé da Silva, A. H., Tempel Stumpf, F., & Marcos Guilherme, C. E. (2022). Evaluation of residual strength of polymeric yarns subjected to previous impact loads. *Acta Polytechnica*, *62*(4), 473–478. https://doi.org/10.14311/AP.2022.62.0473.

Hoss, L. (2009). *Modelos constitutivos hiperelásticos para elastômeros incompressíveis: ajuste, comparação de desempenho e proposta de um novo modelo*. Tese de Doutorado, Universidade Federal do Rio Grande do Sul, Porto Alegre, RS, Brasil. http://hdl.handle.net/10183/16310.

Huang, W., Liu, H., Lian, Y., & Li, L. (2013). Modeling nonlinear creep and recovery behaviors of synthetic fiber ropes for deepwater moorings. *Applied Ocean Research*, *39*, 113-120. https://doi.org/10.1016/j.apor.2012.10.004.

ISO, International Standardization Organization. (2005), *ISO 139: Textiles — Standard atmospheres for conditioning and testing.* Geneva: ISO Publications.

ISO, International Standardization Organization. (2009), *ISO 2062: Textiles — Yarns from packages — Determination of single-end breaking force and elongation at break using constant rate of extension (CRE) tester*. Geneva: ISO Publications.

ISO, International Standardization Organization. (2019), *ISO 18692-2:Fibre ropes for offshore station keeping — Part 2: Polyester*. Geneva: ISO Publications.

ISO, International Standardization Organization. (2020), *ISO 18692-3: Fibre ropes for offshore station keeping — Part 3: High modulus polyethylene (HMPE)*. Geneva: ISO Publications.

Leite, S., & Boesten, J. (2011). HMPE mooring lines for deepwater MODUs. In *Offshore Technology Conference Brasil* (OTC-22486). https://doi.org/10.4043/22486-MS.

Lian, Y., Liu, H., Zhang, Y., & Li, L. (2017). An experimental investigation on fatigue behaviors of HMPE ropes. *Ocean Engineering*, *139*, 237-249. https://doi.org/10.1016/j.oceaneng.2017.05.007.

Liu, H., Huang, W., Lian, Y., & Li, L. (2014). An experimental investigation on nonlinear behaviors of synthetic fiber ropes for deepwater moorings under cyclic loading. *Applied Ocean Research*, *45*, 22-32. https://doi.org/10.1016/j.apor.2013.12.003.

Louzada, E. L. V., Guilherme, C. E. M., & Stumpf, F. T. (2016). Evaluation of the fatigue response of polyester yarns after the application of abrupt tension loads. *Acta Polytechnica CTU Proceedings*, *7*, 76–78. https://doi.org/10.14311/APP.2017.7.0076.

McKenna, H. A., Hearle, J. W., & O'Hear, N. (2004). *Handbook of fibre rope technology* (Vol. 34). Woodhead publishing.

Melito, I., Cruz, D., Belloni, E., Clain, F., & Guilherme, C. (2023). The effects of mechanical degradation on the quasi static and dynamic stiffness of polyester yarns. *Engineering Solid Mechanics*, *11*(3), 243-252. https://doi.org/10.5267/j.esm.2023.4.001.

Mooney, R. (1940). A theory of large elastic deformation. *Journal of Applied Physics*, 11, p. 582-592. https://doi.org/10.1063/1.1712836.

Nguyen, N., & Thiagarajan, K. (2022). Nonlinear viscoelastic modeling of synthetic mooring lines. *Marine Structures*, *85*, 103257. https://doi.org/10.1016/j.marstruc.2022.103257.

Pham, H. D., Cartraud, P., Schoefs, F., Soulard, T., & Berhault, C. (2019). Dynamic modeling of nylon mooring lines for a floating wind turbine. *Applied Ocean Research*, *87*, 1-8. https://doi.org/10.1016/j.apor.2019.03.013.

Rivlin, R. S. (1956). *Rheology Theory and Applications* Vol 1. F. R. Eirich Ed., Academic Press, New York, Ch. 10, p. 351.

Sedighiani, K., Diehl, M., Traka, K., Roters, F., Sietsma, J., & Raabe, D. (2020). An efficient and robust approach to determine material parameters of crystal plasticity constitutive laws from macro-scale stress–strain curves. *International Journal of Plasticity*, *134*, 102779. https://doi.org/10.1016/j.ijplas.2020.102779.

Simo, J. C. & Hughes, T. J. R. (1997), *Computational Inelasticity*. Springer-Verlag, New York, USA.

Sørum, S. H., Fonseca, N., Kent, M., & Faria, R. P. (2023). Assessment of nylon versus polyester ropes for mooring of floating wind turbines. *Ocean Engineering*, *278*, 114339. https://doi.org/10.1016/j.oceaneng.2023.114339.

Sry, V., Mizutani, Y., Endo, G., Suzuki, Y., & Todoroki, A. (2017). Consecutive impact loading and preloading effect on stiffness of woven synthetic-fiber rope. *Journal of Textile Science and Technology*, *3*(1), 1-16. https://doi.org/10.4236/jtst.2017.31001.

Stumpf, F. T., Guilherme, C. E. M., da Cruz, D. M., da Silva, A. H. M. F. T., & Bastos, M. B. (2023). A general constitutive model for the numerical simulation of different synthetic fibres used in offshore mooring. *Ships and Offshore Structures*, *18*(9), 1338-1344. https://doi.org/10.1080/17445302.2022.2116766.

Tang, H. J., Yeh, P. H., Huang, C. C., & Yang, R. Y. (2020). Numerical study of the mooring system failure of aquaculture net cages under irregular waves and current. *Ocean Engineering*, *216*, 108110. https://doi.org/10.1016/j.oceaneng.2020.108110.

Tsukrov, I., Eroshkin, O., Paul, W., & Celikkol, B. (2005). Numerical modeling of nonlinear elastic components of mooring systems. *IEEE Journal of Oceanic Engineering*, *30*(1), 37-46. https://doi.org/10.1109/JOE.2004.841396.

Vlasblom, M., Boesten, J., Leite, S., & Davies, P. (2012). Development of HMPE fiber for permanent deepwater offshore mooring. In *Offshore Technology Conference* (OTC-23333). https://doi.org/10.4043/23333-MS.

Wang, J. J., Wang, C., Fan, J. S., & Mo, Y. L. (2022). A deep learning framework for constitutive modeling based on temporal convolutional network. *Journal of Computational Physics*, *449*, 110784. https://doi.org/10.1016/j.jcp.2021.110784.

Weller, S. D., Johanning, L., Davies, P., & Banfield, S. J. (2015). Synthetic mooring ropes for marine renewable energy applications. *Renewable Energy*, *83*, 1268-1278. https://doi.org/10.1016/j.renene.2015.03.058.

Wibner, C., Versavel, T., & Masetti, I. (2003). Specifying and testing polyester mooring rope for the Barracuda and Caratinga FPSO deepwater mooring systems. In *Offshore Technology Conference* (OTC-15139). https://doi.org/10.4043/15139-MS.

Włochowicz, A., Kukla, S., & Drobina, R. (2016). Static and fatigue strength of linear textile products. *Fibres & Textiles in Eastern Europe*, 24, 3(117), 8-16. https://doi.org/10.5604/12303666.1196606.

Xu, S., Wang, S., & Soares, C. G. (2020). Experimental investigation on hybrid mooring systems for wave energy converters. *Renewable Energy*, *158*, 130-153. https://doi.org/10.1016/j.renene.2020.05.070.

Yuan, Z. M., Incecik, A., & Ji, C. (2014). Numerical study on a hybrid mooring system with clump weights and buoys. *Ocean Engineering*, *88*, 1-11. https://doi.org/10.1016/j.oceaneng.2014.06.002.